Spectroscopic properties of alexandrite crystals

Richard C. Powell, Lin Xi, Xu Gang, and Gregory J. Quarles
Department of Physics, Oklahoma State University, Stillwater, Oklahoma 74078

John C. Walling
Allied Corporation, Mount Bethel, New Jersey 07060

(Received 11 March 1985)

Details of the optical-spectroscopic properties of alexandrite ($BeAl_2O_4:Cr^{3+}$) crystals were studied by different laser-spectroscopy techniques. The temperature dependences of the fluorescence lifetimes and widths of the zero-phonon lines were found to be quite different for Cr^{3+} ions in the mirror and inversion crystal-field sites. The results indicate that direct phonon-absorption processes dominate both thermal line broadening and lifetime quenching for ions in the mirror sites while phonon-scattering processes dominate the line broadening of inversion-site ions and leave their lifetime independent of temperature. Tunable-dye-laser site-selection methods were used to obtain the excitation spectra of the Cr^{3+} ions in inversion sites at low temperature and to identify six types of exchange-coupled pairs of Cr^{3+} ions in the lattice. Time-resolved site-selection spectroscopy was used to monitor the energy transfer between Cr^{3+} ions in mirror and inversion sites at both low and high temperature. Finally, high-power, picosecond pulse excitation was used to produce two-photon absorption, and the resulting emission spectrum was found to exhibit a new fluorescence band in the 400-nm spectral region.

I. INTRODUCTION

Alexandrite ($BeAl_2O_4:Cr^{3+}$) has become technologically important as a tunable solid-state laser material.[1-5] However, the properties of the optical spectra of alexandrite crystals have not been studied in great detail as they have for other important laser materials such as ruby ($Al_2O_3:Cr^{3+}$). The characteristics of the optical spectra provide important information for understanding the fundamental interactions between the optically active ions and the host lattice, and the interactions between two optically active ions. These interactions affect the optical pumping and decay dynamics relevant to the laser operation of the material. We report here the results of a series of different types of laser-spectroscopy measurements on alexandrite which provide new information concerning the crystal-field energy levels, ion-ion interaction, and electron-phonon interaction properties of this material.

The sample used for this investigation was an oriented, single-crystal cube of alexandrite with each edge measuring about 5 mm in length, containing 0.0897 at. % Cr^{3+} ions. The host crystal has the chrysoberyl, hexagonal-close-packed structure shown in Fig. 1.[6] The space group is orthorhombic *Pnma* with four molecules per unit cell and lattice parameters $a=9.404$ Å, $b=5.476$ Å, and $c=4.427$ Å. The Al^{3+} ions are octahedrally coordinated by the oxygen ions and occur in two inequivalent crystal-field sites in this lattice. The Al^{3+} sites lying in the mirror-symmetry planes of the lattice have the site symmetry of the C_s point group, while the other Al^{3+} sites possess inversion symmetry and belong to the C_i point group. The Cr^{3+} ions enter the crystal substitutionally for the Al^{3+} ions, 78% replacing Al^{3+} ions in the mirror sites and the rest going into the inversion sites.[7,8]

The energy-level diagram for Cr^{3+} ions in the mirror sites is shown in Fig. 2. The six oxygen ligands produce a crystal field which can be described as having O_h point-

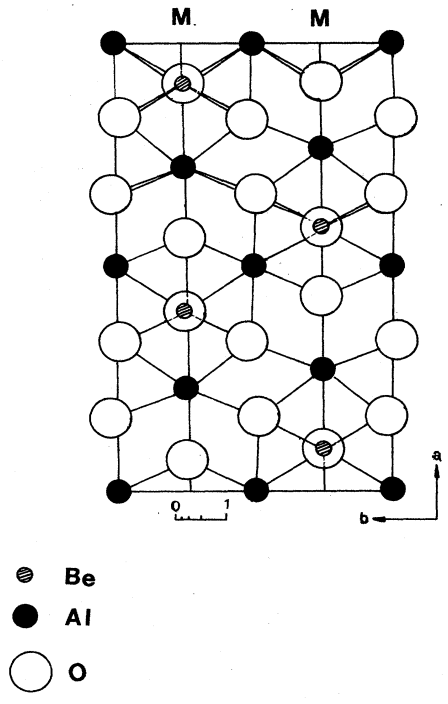

FIG. 1. *c*-axis view of chrysoberyl structure (from Ref. 6). *M* denotes mirror planes.

group symmetry slightly distorted to C_s. The O_h crystal field splits the free-ion wave functions of the $3d^3$-electron configuration of the Cr^{3+} ion into crystal-field wave functions having t^3- or t^2e-electron configurations, and either quartet or doublet multiplicities depending on the spin alignments of the electrons. The distortion to C_s symmetry causes a splitting of all of the orbitally degenerate T and E levels but not the orbital singlet A levels. Note that in performing the reduction from O_h to C_s symmetry it is important to take the diagonal mirror plane of the cube as the mirror element in the C_s group. The spin-orbit interaction of the electrons causes further splitting, leaving all levels designated as S_1,S_3 Kramers degenerate doublets.

Figure 2 also shows the electric-dipole-allowed absorption transitions. Since all transitions within states of the $3d^3$-electronic configuration are parity forbidden, crystal-field admixing with odd-parity configurations is required for any electric dipole transitions to be observed. These group-theoretical considerations are useful in understanding the qualitative features of the optical spectra, such as the number of lines and their relative intensities for different polarizations. A similar analysis of the ions in the inversion sites with C_i symmetry gives all A_g levels with no specific selection rules.

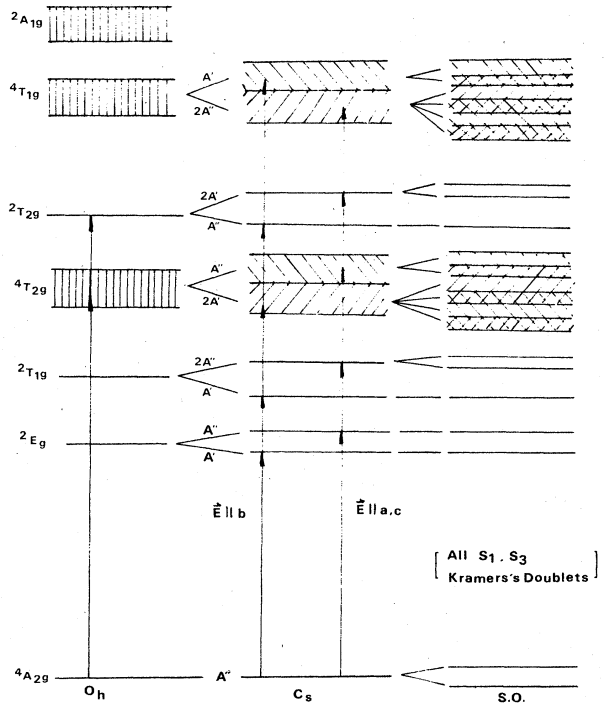

FIG. 2. Energy-level diagram for Cr^{3+} ions in mirror sites in alexandrite. Arrows show absorption transitions allowed by orbital-symmetry selection rules. All transitions between levels of the same parity require crystal-field admixture of levels of opposite parity, and all transitions between levels of different spin multiplicity require spin-orbit interaction to occur.

II. ABSORPTION, FLUORESCENCE, AND EXCITATION SPECTRA

Figure 3 shows the absorption spectra at room temperature. The absorption features consist of two broadbands centered at about 420 and 580 nm, three sets of sharp lines centered near 680, 650, and 470 nm, and the band edge appearing below 300 nm (not shown in the figure). The two bands are associated with transitions from the $^4A_{2g}$ ground state to the $^4T_{2g}$ and $^4T_{1g}$ excited states. These transitions involve changes in the crystal-field orbitals of the electrons and thus are highly sensitive to the crystal-field environment of the ion. Vibrational modulation of the field strength produces the broadbands. The 400-nm band peaks at higher energy and the 580-nm band peaks at lower energy for the **E**||**b** polarization compared to the peak positions for the **E**||**a**,**c** polarization directions. This is consistent with the selection rules and the level-splitting assignments for C_s symmetry shown in Fig. 2.

The three sets of sharp lines are associated with transitions from the ground state to the split components of the ^2E_g (R lines), $^2T_{1g}$ (S lines), and $^2T_{2g}$ (B lines) levels. These involve spin flips of the electron wave functions without changes in crystal-field states. Thus they are insensitive to vibrational modulation of the crystal field and therefore appear as sharp lines. The lines seen in Fig. 3 are associated with mirror-site ions. With the relatively low resolution of the spectra shown in the figure, it is difficult to ascertain the changes in intensity with different polarization for specific lines within a group. Results of this type for the R lines have been reported previously in Ref. 1 and are shown in the inset in Fig. 3. They show that the intensity of the transition to the lower component of the split ^2E_g level (R_{1m}) is significantly greater than the intensity of the transition to the upper component (R_{2m}) for **E**||**b** polarization, and these relative intensities are reversed for the other two polarization directions. These results are consistent with the polarization selection rules shown for the R lines in Fig. 2.

The lines associated with the inversion-site ions are very

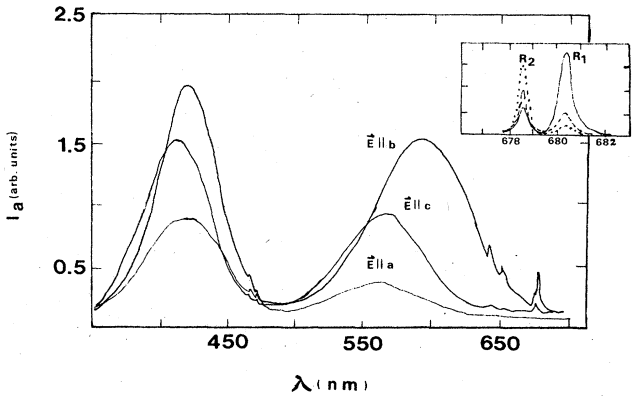

FIG. 3. Absorption spectra of alexandrite at room temperature. Inset shows R_m lines from Ref. 1. Solid line for **E**||**b**; dotted line for **E**||**c** with sensitivity ×4; dashed line for **E**||**a** with sensitivity ×40.

weak and difficult to observe in the absorption spectra and the broad absorption bands are hard to resolve from those associated with mirror-site ions. Some of the properties of transitions of ions in inversion sites obtained from other types of spectral measurements are discussed below. Polarization changes have been used to identify these as magnetic dipole transitions.[1]

The fluorescence emission at room temperature is shown in Fig. 4 for three excitation wavelengths. The major features of the spectra are the two sharp lines R_{1m} and R_{2m} and the broad, structured band peaking at lower energies. The latter is due the superposition of low-energy vibronic emission transitions from the components of the ^2E_g level and emission from the relaxed excited state of the $^4T_{2g}$ level which is Stokes-shifted to lower energy compared to the absorption transition involving this level. The structure in this sideband is a mixture of specific one-phonon vibronic peaks, and zero-phonon lines associated with transitions from the $^4T_{2g}$ and $^2T_{1g}$ levels. Tentative assignments have been made for the S_m lines,[1] but the other peaks have not been identified since no complete analysis of vibronic transitions has been done for Cr^{3+} ions in $BeAl_2O_4$ crystals. For certain excitation wavelengths, the R_{1i} and R_{2i} lines associated with Cr^{3+} ions in inversion sites can also be seen.

The spectra shown in Fig. 4 represent the E||b polarization direction. For the other two polarization directions the broad emission band is significantly smaller in intensity relative to the R_m lines.[1] This is consistent with the absorption-band positions shown in Fig. 3 and with the crystal-field splittings and selection rules shown in Fig. 2 for the transitions involving the $^4T_{2g}$ level. The E||b polarization involves allowed vibronic emission from the lowest crystal-field component of the split $^4T_{2g}$ level, which will have the greatest degree of occupancy in thermal equilibrium. The other two polarization directions have forbidden transitions from this component and allowed transitions from the higher component, which has a lower degree of occupancy. The observed fluorescence intensity will depend both on the selection rules and the degree of occupancy of the initial level of the transition.

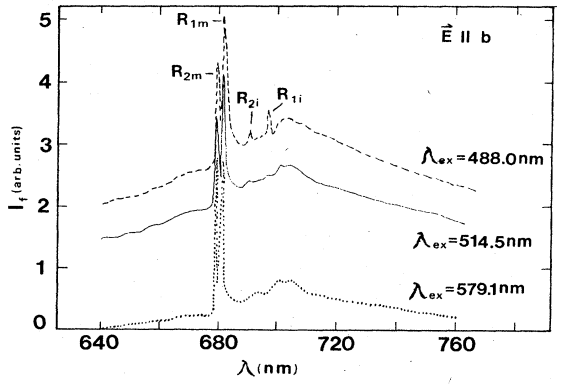

FIG. 4. Fluorescence spectra of alexandrite at room temperature.

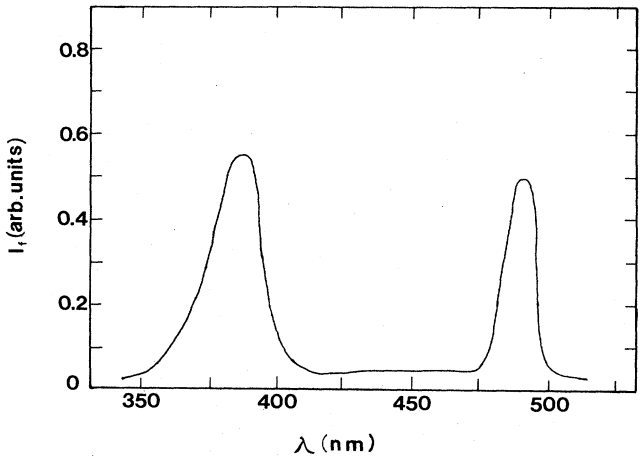

FIG. 5. Excitation spectrum of R_{1i} line of alexandrite at room temperature.

The excitation spectra of the R_{1m} and R_{1i} lines are shown in Figs. 5 and 6. The spectrum for the mirror-site emission at room temperature is essentially the same as the absorption spectrum shown in Fig. 3. The two excitation bands for the inversion-site ions are seen in Fig. 5 to peak near 480 and 380 nm. The expanded spectral region shown in Fig. 6 at room temperature shows very different excitation characteristics for the ions in the two types of sites. This indicates that energy transfer between ions in the two nonequivalent types of sites is very weak for the

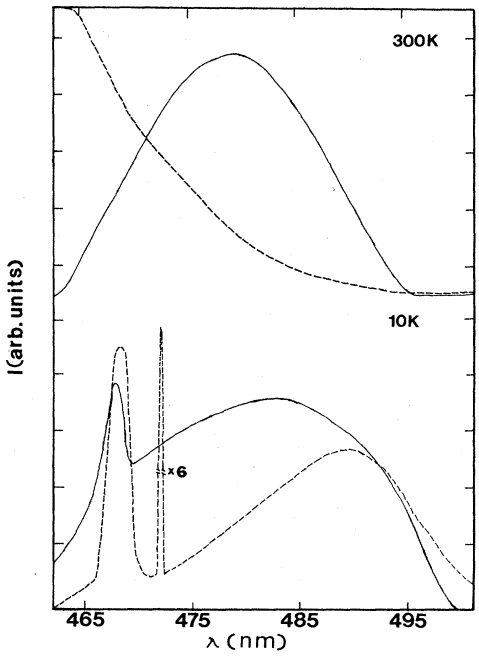

FIG. 6. Excitation spectra of the R_1 lines of alexandrite in the spectral region between the major absorption bands at 300 and 10 K. The solid line is for the R_{1i} line and the dashed line is for the R_{1m} line.

chromium concentration level in this sample. The spectral features shown for these conditions are similar to those reported recently by Schepler.[9] The spectral features in this region change substantially as temperature is lowered to 10 K. A set of sharp lines appears which can be associated with the B_m lines and attributed to transitions terminating on the split components of the $^2T_{2g}$ level of ions in mirror sites. Also, ions in both mirror and inversion sites exhibit a similar excitation band in this spectral region. Since this is known from room-temperature results to be the region of inversion-site absorption, the results indicate the presence of energy transfer from ions in inversion sites to ions in mirror sites. This is discussed further in Sec. IV.

The final experiment on the absorption and fluorescence spectra of $BeAl_2O_4:Cr^{3+}$ involved monitoring the fluorescence emission occurring after two-photon—absorption excitation. A 30-ps pulse from a frequency-doubled Nd-YAG laser (YAG denotes yttrium-aluminum-garnet) at 532 nm polarized parallel to the b direction was used for excitation. This has weak single-photon absorption by mirror-site ions in the visible spectral region and strong two-photon absorption in the uv region terminating on a shoulder of the band edge as seen in Fig. 7. The fluorescence observed after this type of excitation occurs in two regions: the normal emission in the 700-nm region as shown in Fig. 4 and a new emission band in the 400-nm region as shown in Fig. 7. This new, broad, structured emission band has not been reported previously and may be important in determining the excited-state absorption and dispersion properties of the material.

The broad luminescence band near 400 nm may be due to a $^2A_{1g}$-$^4A_{2g}$ transition. The initial state of this transition is a Stokes-shifted upper level of the $t_{2g}^2e_g$-electron configuration. The reciprocal transition in absorption should be a broadband shifted to higher energies. However, it is difficult to observe because it is both spin and symmetry forbidden in O_h symmetry and thus will be a very weak, broadband on the tail of the absorption edge. The absorption-edge shoulder at higher energies is probably due to a charge-transfer transition. The structure observed in the band cannot be explained by crystal-field or spin-orbit splitting and may be due to the effects of radiative reabsorption by the $^4T_{1g}$ band.

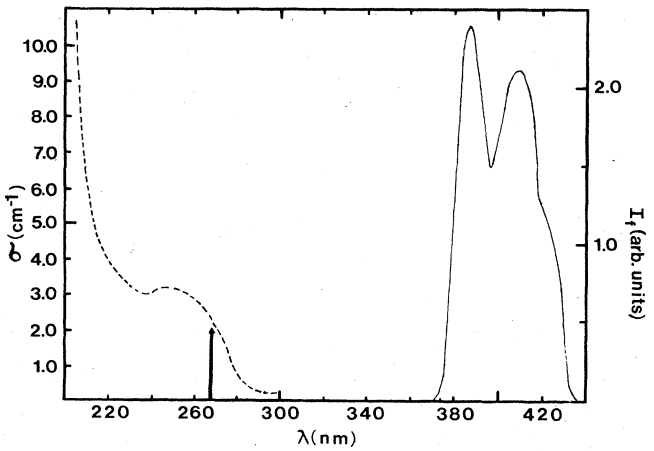

FIG. 7. Fluorescence emission in the 400-nm spectral region of alexandrite after two-photon excitation with a 30-ps pulse at 532 nm at room temperature. The dashed line shows the absorption-band edge (**E**||**b**; sample thickness 0.6 cm) with the arrow at 266 nm showing the region excited by the two-photon transition.

III. SPECTRAL EFFECTS OF ELECTRON-PHONON INTERACTIONS

Lattice vibrations interact with the electronic energy levels and transitions of the Cr^{3+} ions through the modulation of the local crystal field. The results of this interaction manifest themselves in the optical spectral properties through the initiation of vibronic transitions, radiationless transitions, and phonon-scattering mechanisms. The first of these produces the broad spectral bands described in the preceding section. The second leads to a temperature-dependent decrease of the fluorescence lifetime of the R lines and both the second and third can cause a thermal broadening of the R lines. The measurement of these last two effects are discussed in this section.

A. Fluorescence lifetimes

Figure 8 shows the temperature dependences of the fluorescence lifetimes of the R lines for Cr^{3+} ions in both mirror and inversion sites. The lifetime of the emission of the ions in the mirror sites decreases from about 2.3 ms at 10 K to about 290 μs at 300 K. The long lifetime at low

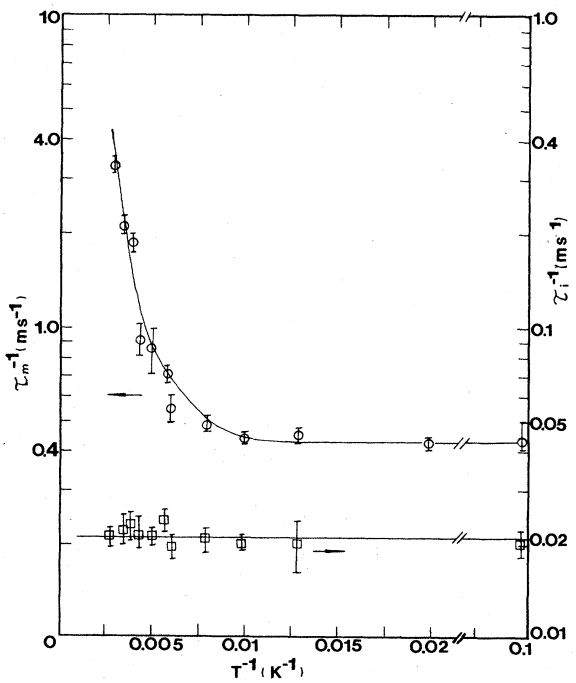

FIG. 8. Temperature dependences of the fluorescence decay times of Cr^{3+} ions in mirror and inversion sites in alexandrite. The solid lines represent the best fits to the data using Eq. (1).

temperatures is the intrinsic lifetime of the ^2E_g state for ions in this type of site, while the reduced lifetime at high temperatures is due to thermal excitation to higher-lying levels with shorter intrinsic decay times. This quenching can be modeled by considering two excited levels in thermal equilibrium with intrinsic decay rates τ_E^{-1} and τ_T^{-1}. The common decay rate of the coupled levels is given by

$$\tau^{-1}=\tau_E^{-1}+\tau_T^{-1}\exp(-\Delta E_Q/k_BT)\ , \tag{1}$$

where ΔE_Q is the splitting between the two levels and k_B is the Boltzmann constant. The solid line in Fig. 8 is the best fit to the data treating ΔE_Q and τ_T as adjustable parameters. The results give the energy-level splitting as 800 cm^{-1} and the lifetime of the upper level as 7.1 μs.

The inversion-site emission has a lifetime of about 48 ms and shows no change with temperature. The long lifetime is consistent with the forbidden nature of these transitions, and the lack of temperature dependence is consistent with the spectral observation that the upper energy levels are shifted to higher energy compared to the mirror sites, thus minimizing quenching of the ^2E_g levels through thermal-excitation processes to these higher levels.

The fluorescence lifetime of the broadband emission from Cr^{3+} ions in the mirror sites is the same after two-photon excitation, but the rise time of the fluorescence is measured to be about 20 μs. The broadband emission around 400 nm has a decay time of about 8 μs with a negligible rise time. The measured fluorescence lifetime of the 400-nm band is significantly shorter than expected for a spin-forbidden radiative transition which may indicate quenching due to radiationless relaxation. This is consistent with the observed rise time of the 700-nm emission after two-photon excitation, which implies the presence of an indirect pumping process of the normal fluorescence transitions. If this is due to relaxation from the 400-nm level, the rise time should be given by

$$t_r=(\tau_E^{-1}-\tau_{400\ nm}^{-1})^{-1}\times\ln\{(\tau_{400\ nm}/\tau_E)\times[1-(\tau_E^{-1}-\tau_{400\ nm}^{-1})\tau_{nr}N_E/N_{400\ nm}]\}\ . \tag{2}$$

Here, τ_{nr} is the nonradiative decay time of the upper level, while N_E and $N_{400\ nm}$ are the initial populations of the upper and lower level, respectively. Use of the measured fluorescence lifetimes with no direct pumping of the ^2E level results in a predicted value of 30 μs for t_r. The slightly shorter observed value can be attributed to the presence of some pumping of the ^2E_g level through one-photon—absorption processes to the $^4T_{2g}$ band. Setting $\tau_{nr}N_E/N_{400\ nm}=17.94$ μs in Eq. (2) gives the observed result.

B. Linewidths

Electron-phonon processes also cause a temperature dependence of the widths of spectral lines. The width of a zero-phonon transition can have contributions from variations in the local static crystal field, direct phonon transitions, and Raman scattering of phonons. The first of these results in a temperature-independent Gaussian contribution to the linewidth due to inhomogeneous broadening. The second is a lifetime-broadening process which produces a temperature-dependent Lorentzian line shape. The third mechanism also gives a temperature-dependent Lorentzian contribution to the linewidth.

The temperature dependences of the full widths at half maximum of the R_1 lines from Cr^{3+} ions in mirror and inversion sites are shown in Fig. 9. Both lines approach a constant value at low temperature and broaden rapidly at high temperature. This is similar to the thermal broadening of the R lines in ruby.[10,11] The low-temperature linewidth is the inhomogeneous contribution due to local strains, while the temperature variation can be interpreted as being due to phonon-scattering processes and direct phonon transitions. In the Debye approximation the expression for line broadening due to Raman scattering of phonons is[12]

$$\Delta\nu=(\omega_D/4\pi^2)\int_0^1 dx\ \ln\{1+9\pi^2W^2x^6\exp(xT_D/T)[\exp(xT_D/T-1)]^{-2}[g^2(x)+(9\pi^2/4)W^2x^6]^{-1}\}\ , \tag{3}$$

where

$$g(x)=1+W\{1+3x^2+1.5x^3\ln[(1-x)/(1+x)]\}\ . \tag{4}$$

The Debye temperature and frequency are given by T_D and ω_D, respectively, while W is the quadratic electron-phonon coupling constant. Using either velocity-of-sound measurements[3] or specific-heat data,[13] the Debye temperature for $BeAl_2O_4$ can be estimated and is found to be approximately 500 K.

The linewidth contribution due to a direct-phonon-absorption process is given by

$$\Delta\nu=\sum_i \beta_i\{\exp[(\Delta E_i/k_BT)-1]\}^{-1}\ , \tag{5}$$

where ΔE_i is the energy-level splitting spanned by the phonon process and β_i is the coupling constant. The total broadening due to this type of process is the sum over all possible phonon transitions.

Attempts were made to use Eqs. (3) and (5) to fit the measured temperature-dependent widths of the R_1 lines after subtracting the low-temperature residual linewidths. For R_{1i} a good fit was obtained using Eq. (3) with values for W of either 0.79 or -0.2. This is shown as a solid line in Fig. 9. The perturbation-theory approach used in Ref. 10 gives an equally good fit to the data, but the value of the coupling coefficient does not justify use of the weak-coupling limit.

A good fit to the inversion-site data after subtracting the inhomogeneous contribution to the linewidth can also be obtained using Eq. (5) and treating β and ΔE as adjustable parameters. This is shown by a dotted line in the fig-

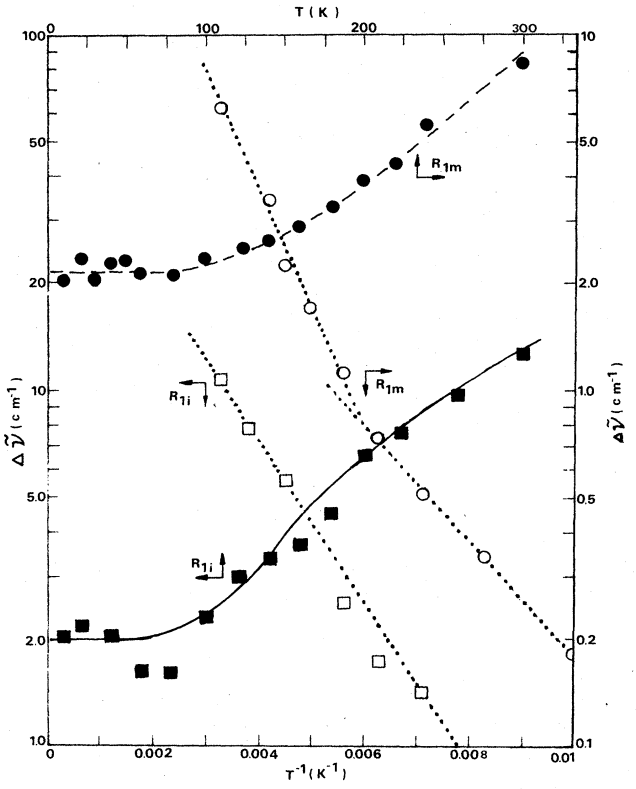

FIG. 9. Temperature dependences of the full widths at half maximum of the R_1 lines in alexandrite. Circles are for R_{1m} and squares are for R_{1i} lines; solid symbols are measured data and open symbols represent the linewidths after subtraction of the temperature-independent inhomogeneous contributions. The solid line represents theoretical fit to the data using Eq. (3), while the dotted lines represent the best fits using Eq. (5). The parameters giving these fits are listed in Table I. The dashed line shows the general trend in the data and does not represent a theoretical fit.

ure with $\beta=59$ cm^{-1} and $\Delta E=365$ cm^{-1}. Since this activation energy does not correspond to a known splitting between inversion-site energy levels, it is concluded that the Raman scattering processes dominate the homogeneous line broadening for ions in the inversion sites.

No good fit to the data obtained on the temperature dependence of the linewidth for the R_{1m} line could be found using Eq. (3). After subtracting the inhomogeneous contribution to the linewidth of 2.15 cm^{-1}, the data can be fitted using Eq. (5) with two terms in the sum as shown by the dotted lines in Fig. 9. The first process has a coupling constant of 8 cm^{-1} and an energy splitting of 264 cm^{-1}, while $\beta=202$ cm^{-1} and $\Delta E=800$ cm^{-1} for the second process. The latter is consistent with direct phonon absorption to the $^4T_{2g}$ level, while the former may be associated with transitions to the components of the $^2T_{1g}$ levels.

The parameters obtained from these lifetime and linewidth measurements are summarized in Table I.

IV. ION-ION INTERACTION

The Cr^{3+} ions in the lattice can interact with each other through various electric or magnetic multipole interactions or through exchange. The mechanism for the interaction depends on the spacing and geometric arrangement of the ion pairs. Weak interaction can be treated as energy transfer between two isolated Cr^{3+} ions, whereas strong interaction produces coupled pairs with energy levels and transitions much different than those of isolated ions. In materials such as ruby it has been found that both types of interactions are present,[14–16] and we have observed both types of interactions in alexandrite crystals, as described below.

A. Energy transfer between Cr^{3+} ions

Site-selection time-resolved spectroscopy methods were used to investigate the transfer of energy from Cr^{3+} ions in mirror sites to Cr^{3+} ions in inversion sites. A 10-ns dye-laser pulse tuned to near 475 nm was used to selectively excite a nonequilibrium distribution of the ions in the two types of sites, and the time evolution of the fluorescence spectrum was monitored using a 1-m monochromator, an RCA C31034 photomultiplier tube, and an EGG-PAR boxcar integrator. Figure 10 shows the variation of the ratios of the integrated fluorescence intensities of the R_1 emission lines of Cr^{3+} ions in inversion and mirror sites as a function of time after the laser-excitation pulse at 10 K and room temperature.

The observed energy-transfer characteristics can be explained by assuming that the dominant transfer takes place from the ions in the higher-energy mirror sites to the ions in the lower-energy inversion sites with no back transfer. The time evolution of the sensitizer fluorescence intensity is described by an expression derived by Inokuti and Hirayama,[17] while the expression for the time evolution of the activator fluorescence intensity has been derived by Huber.[18] Assuming electric-dipole–dipole interaction, the ratio of these expressions has the form

$$I_i(t)/I_m(t)=At^{-1/2}\exp(Bt^{1/2}) , \tag{6}$$

where

$$B=(4\pi^{3/2}/3)N_i\alpha^{1/2} , \tag{7}$$

and A is a constant factor involving the radiative decay rates and initial concentrations of the ions in the two types of sites. The energy-transfer parameter can be expressed in terms of the critical interaction distance R_0 as

$$\alpha=R_0{}^6/\tau_m . \tag{8}$$

The dashed and solid lines in Fig. 10 show the best fits to the data found by using Eq. (6) and treating A and B as adjustable parameters. At room temperature a reasonable fit is obtained for an energy-transfer parameter of $\alpha=6.1\times10^{-36}$ cm^{6}sec^{-1}. This implies a critical interaction distance of 35 Å. At low temperature the general shape of the time evolution of the fluorescence intensity ratios can be predicted by Eq. (6), but the data cannot be fitted exactly. The best simultaneous fit to the long-time and short-time parts of the data is shown in the figure.

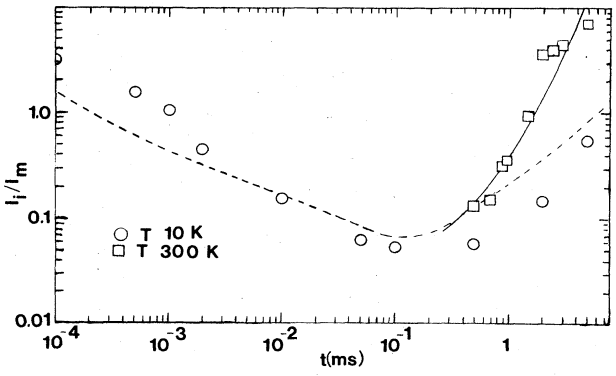

FIG. 10. Evolution of the ratios of the integrated fluorescence intensities of the R_1 lines in mirror and inversion sites as a function of time after the laser-excitation pulse at 300 and 10 K. The solid and dashed lines represent the best fits to the data using Eq. (6) with the parameters listed in Table I.

This was obtained using an energy-transfer parameter of $\alpha=1.9\times10^{-36}$ cm^{6}sec^{-1}, which implies a critical energy-transfer distance of 40 Å. The poor fit to the data indicates that the simple model used for this interpretation is not adequate at low temperatures. The major difficulty is probably associated with the presence of a nonstatistically random distribution of Cr^{3+} ions as discussed in the following part of this section. The energy-transfer parameters obtained from fitting these time-resolved—spectroscopy data are summarized in Table I.

B. Exchange-coupled pairs of Cr^{3+} ions

When the chromium ions are located close enough to each other to interact strongly, they produce satellite lines in the optical spectra called N lines. Figure 11 shows the region of the fluorescence spectrum near the R_m lines for several different excitation wavelengths in this region. The tunable dye laser was used for excitation and an EGG-PAR optical multichannel analyzer (OMA) was used for data acquisition. The observed spectral lines can be attributed to transitions between levels of exchange-coupled pairs of Cr^{3+} ions. This type of pair spectrum has been observed for Cr^{3+} ions in other hosts.[16,19,20]

The interaction Hamiltonian describing the exchange coupling of the chromium ion pairs is

$$H_{ex}=-JS_1\cdot S_2\ , \tag{9}$$

where the coupling constant J is positive for ferromagnetic coupling and negative for antiferromagnetic coupling. The ground-state energy-level splitting due to ferromagnetic exchange coupling for two Cr^{3+} ions with spin $\frac{3}{2}$ is $\Delta E=0,1J,3J,6J$. For antiferromagnetic coupling of these ions the splitting is $\Delta E=0,3J,5J,6J$. The spectra in Fig. 11 can be associated with the energy-level diagrams of six different types of pairs shown in Fig. 12. Two are ferromagnetically coupled and four antiferromagnetically coupled. The small discrepancies in some of the observed

TABLE I. Summary of alexandrite spectral parameters.

Lifetime data	
τ_{Rm}(10 K)=2.3 ms	τ_{Rm}(300 K)=290 μs
$\Delta E_Q=800$ cm^{-1}	$\tau_T=7.1$ μs
$\tau_{Ri}=48$ ms (all temperatures)	
$\tau_{400\ nm}$(300 K)=8 μs	$t_r=20$ μs

Linewidth data	
Mirror site	Inversion site
$\Delta\nu_0=2.15$ cm^{-1}	$\Delta\nu_0=2.00$ cm^{-1}
$\beta_1=8.0$ cm^{-1}	$T_D=500$ K
$\Delta E_1=264$ cm^{-1}	$W=0.79$ or -0.2
$\beta_2=202$ cm^{-1}	
$\Delta E_2=800$ cm^{-1}	

Energy transfer	
$T=300$ K	$T=10$ K
$\alpha=6.08\times10^{-36}$ cm^{6}sec^{-1}	$\alpha=1.90\times10^{-36}$ cm^{6}sec^{-1}
$R_0=35$ Å	$R_0=40$ Å

Exchange-coupled pairs	
$J_1=4.3$ cm^{-1}	$J_4=4.3$ cm^{-1}
$J_2=-6.2$ cm^{-1}	$J_5=-7.3$ cm^{-1}
$J_3=-6.5$ cm^{-1}	$J_6=-4.4$ cm^{-1}

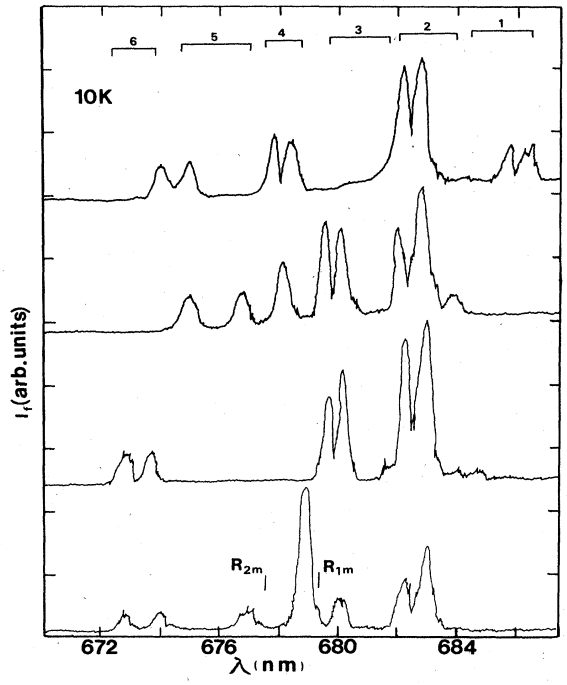

FIG. 11. Fluorescence spectra of N lines in alexandrite at 10 K for four different laser-excitation wavelengths between 670 and 680 nm.

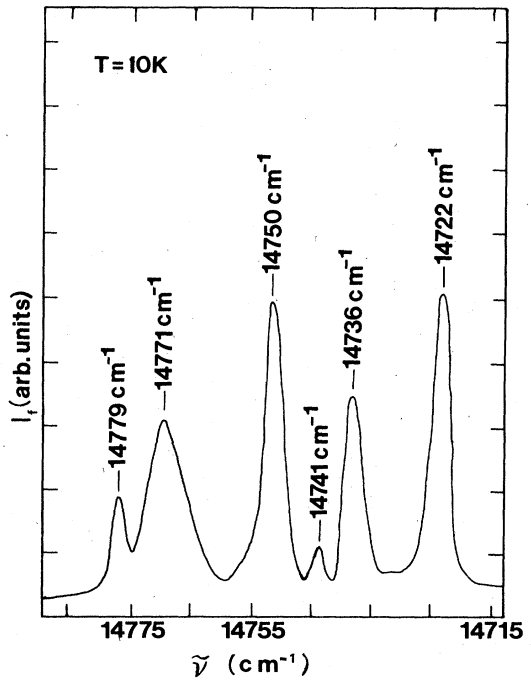

FIG. 13. Excitation spectrum of the pair line at 683 nm in alexandrite at 10 K.

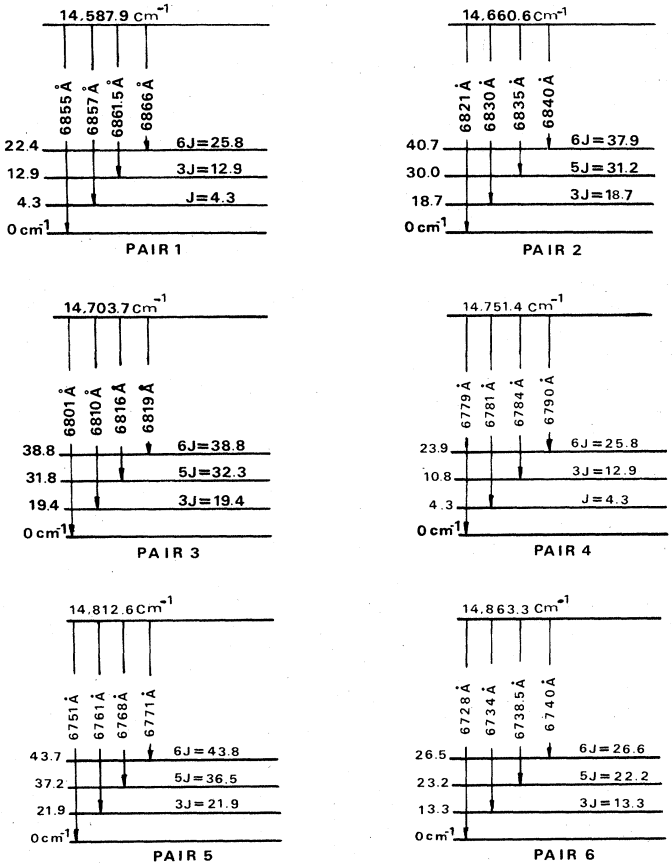

FIG. 12. Energy-level diagrams established for six exchange-coupled pairs of Cr^{3+} ions in alexandrite. The values for the coupling parameter J are listed in Table I.

energy-level values and those predicted by Eq. (9) may be due to effects of "superexchange" or "biquadratic exchange."[16] Table I gives the coupling parameter for each type of pair.

Figure 13 shows the excitation spectrum of the 683-nm pair line as an example of the excited-state splittings. This complex spectrum does not obey any simple splitting progression as seen in the ground-state manifold, and thus no attempt was made to establish excited-state energy-level diagrams for the pairs. The problem may be associated with a breakdown of the ion-ion interaction Hamiltonian given by Eq. (9) when the ions are in the excited state. A Hamiltonian coupling the spins of the individual electrons may be more appropriate in this case.[16]

It is difficult to identify the exact lattice sites involved in these different pairs without extensive investigation using tools such as electron paramagnetic resonance and uniaxial stress.[19] However, the lattice structure of chrysoberyl shown in Fig. 1 provides a variety of different combinations of close-neighbor pair sites involving both mirror and inversion locations.

V. DISCUSSION

The results of the group-theoretical analysis of the energy levels and selection rules for electric dipole transitions for Cr^{3+} ions in the mirror sites in alexandrite crystals presented in Sec. I provide an understanding of the changes in relative intensities and apparent peak positions of the sharp lines and broadbands seen in the absorption and fluorescence spectra for different polarization direc-

tions. The observation of the 400-nm emission band and its excitation through two-photon absorption terminating at 266 nm demonstrates the presence of several higher-lying levels in alexandrite crystals which have also been seen by other types of measurements. For example, the absorption-band edge in Cr^{3+}-doped $BeAl_2O_3$ is shifted toward the visible compared to that of the undoped material. Also, the magnitude of the refractive index change in alexandrite induced by four-wave mixing could be theoretically explained only by assuming the existence of high-oscillator-strength transitions to levels in the ultraviolet spectral region.[21] In addition, excited-state absorption measurements on alexandrite[4,22] show the presence of energy levels in the vicinity of 32 000 cm^{-1}, which is between the absorbing and emitting levels associated with two-photon-excited fluorescence. The properties of these near-uv spectral transitions constitute an important area for future investigation.

The temperature-dependent variations in the spectral properties show the importance of electron-phonon interactions in determining the spectral dynamics of alexandrite. Direct-phonon-absorption processes dominate the temperature dependence of the R_{1m} zero-phonon line. The splitting of the ^2E_g and $^4T_{2g}$ energy levels ($\Delta E_Q = 800$ cm^{-1}) is small enough to be connected by direct-phonon-absorption process. This produces a temperature-dependent lifetime quenching and homogeneous line broadening. Similar phonon processes terminating on the $^2T_{1g}$ level contribute to the line broadening but not to the lifetime quenching. Recent results on the pressure dependence of the alexandrite mirror-site spectra have also been interpreted in terms of direct phonon processes to the $^4T_{2g}$ level for both line broadening and lifetime quenching.[23] It is interesting that no contribution to the line broadening due to Raman scattering of phonons is observed for the R_{1m} line.

The R_{1i} zero-phonon linewidth and lifetime are not affected by direct-phonon-absorption processes in the temperature range investigated because of the large excited-state splittings of the energy levels. Consequently, the lifetime is independent of temperature and the thermal line broadening is dominated by the Raman scattering of phonons.

The temperature variations of the homogeneous linewidths of the R_1 lines in alexandrite are similar to those observed for Cr^{3+} ions in ruby.[10,11,24,25] Contributions to the linewidth have been observed both from Raman scattering processes and from direct phonon processes between the excited-state levels.[11,21,22] The inhomogeneous linewidths observed at low temperatures in alexandrite are greater than those observed for ruby with equivalent Cr^{3+} concentrations. This indicates less random crystal-field environments in ruby than in alexandrite crystals.

The Cr^{3+} ions in alexandrite can interact to form exchange-coupled pairs. In this case the Cr^{3+} ions lose their individual identity and produce absorption and emission spectral lines associated with the energy levels of the pairs. The positions of the emission lines establish the splittings of the ground-state energy levels of each type of pair. The observed splitting progressions of the pair manifolds are consistent with the predictions of the direct-exchange expressions given in Eq. (9). The values of J found for these alexandrite pairs are smaller than most of those reported for ruby and $YAlO_3$ hosts.[16,19,20] This may be due to differences in the pair geometries for the different host crystals or in the exact details of the exchange interaction involving contributions from superexchange or biquadratic exchange effects.[16] In studies of Cr^{3+} exchange-coupled pairs in ruby, it was found that the excited-state splittings are better described by an interaction Hamiltonian involving a summation over all individual electron spin-spin interactions instead of the total ion spin-spin interaction given by Eq. (9). This is probably also true for the pairs in alexandrite, but verification of this will require further work.

The presence of strongly coupled ion pairs complicates the interpretation of energy transfer between mirror- and inversion-site ions which are not strongly coupled. The fact that the Cr^{3+} ions in mirror and inversion sites have distinctly different excitation spectra at room temperature but not at low temperature is consistent with the results of time-resolved site-selection spectroscopy measurements which show very different energy-transfer characteristics at the two temperatures. The different excitation spectra explain why it was possible to establish laser-induced Cr^{3+} population gratings separately for the mirror- and inversion-site ions in alexandrite at room temperature.[21] Both excitation-spectra measurements and time-resolved site-selection spectroscopy results show that energy transfer from ions in inversion sites to ions in mirror sites takes place more strongly at low temperatures.

Normal assumptions concerning energy transfer between randomly distributed sensitizer and activator ions are not strictly valid for Cr^{3+} ions in alexandrite crystals because there is a region around each sensitizer within which strong coupling produces pair spectra instead of energy transfer. Thus the values of R_0 obtained from fitting Eq. (6) to time-resolved spectroscopy results should only be considered as effective interaction distances for comparing energy-transfer characteristics at different concentrations, temperatures, etc. The values listed in Table I are significantly larger than predicted from spectral overlap considerations assuming a uniform distribution of Cr^{3+} ions.[26] The apparent increase in energy transfer at low temperature is somewhat surprising since lowering the temperature generally quenches energy transfer instead of enhancing it. For the case of alexandrite it appears that the interaction causing the strong coupling decreases more at low temperature than the value of R_0 for energy transfer. This decreases the size of the strong-coupling sphere surrounding each sensitizer and allows activator ions closer to the excited sensitizer to take part in energy transfer instead of forming coupled pairs. Although this reasoning can account for the observed change in energy transfer with temperature, it is obviously a simplified picture of a very complex situation for ion-ion interaction in alexandrite.

The performance of alexandrite as a tunable solid-state laser material is critically dependent on the spectral dynamics of the Cr^{3+} ions. The two types of spectral information reported here most relevant to laser characteris-

tics concern the near-uv spectral bands and the ion-ion interaction. The former can contribute to degradation of lasing operation through excited-state absorption and nonlinear optical effects. The latter shows the importance of having a uniform distribution of Cr^{3+} ions in the crystal to minimize the presence of exchange-coupled pairs which do not contribute to laser emission. In addition, Cr^{3+} ions in inversion sites do not have the same lasing properties as ions in mirror sites and thus energy transfer from the mirror-site ions to inversion-site ions alters the laser operation. Therefore it is important to minimize the percentage of Cr^{3+} ions in inversion sites, which might be done through co-doping with ions which preferentially occupy these sites.

ACKNOWLEDGMENTS

This research was sponsored by the U.S. Army Research Office (Durham, NC), Department of the Army, and by the National Science Foundation under Grant No. DMR-82-16551.

[1]J. C. Walling, O. G. Peterson, H. P. Jenssen, R. C. Morris, and E. W. O'Dell, IEEE J. Quantum Electron. **QE-16**, 1302 (1980); J. C. Walling and O. G. Peterson, *ibid.*, 119 (1980).

[2]J. C. Walling, H. P. Jenssen, R. C. Morris, E. W. O'Dell, and O. G. Peterson, Opt. Lett. **4**, 182 (1979).

[3]C. F. Cline, R. C. Morris, M. Dutoit, and P. J. Harget, J. Mater. Sci. **14**, 941 (1979).

[4]M. L. Shand, J. Appl. Phys. **54**, 2602 (1983); M. L. Shand, J. C. Walling, and R. C. Morris *ibid.* **52**, 953 (1981).

[5]B. K. Sevast'Yanov, Yu. I. Remigailo, V. P. Orekhova, V. P. Matrosov, E. G. Tsvetkov, and G. V. Bukin, Dokl. Akad. Nauk SSSR **256**, 373 (1981) [Sov. Phys.—Dokl. **26**, 62 (1981)].

[6]E. F. Farrell, J. H. Fang, and R. E. Newnham, Am. Mineral. **48**, 804 (1963); E. F. Farrell and R. E. Newnham, *ibid.* **50**, 1972 (1965).

[7]R. E. Newnham, R. Santoro, J. Pearson, and C. Jansen, Am. Mineral. **449**, 427 (1964).

[8]M. L. Shand, J. C. Walling, and H. P. Jenssen, IEEE J. Quantum Electron. **QE-18**, 167 (1982).

[9]K. L. Schepler, J. Appl. Phys. **56**, 1314 (1984).

[10]D. E. McCumber and M. C. Sturge, J. Appl. Phys. **34**, 1682 (1963).

[11]R. C. Powell, B. DiBartolo, B. Birang, and C. S. Naiman, J. Appl. Phys. **37**, 4973 (1966).

[12]D. Hsu and J. L. Skinner, J. Chem. Phys. **81**, 5471 (1984).

[13]*Specific Heat of Nonmetallic Solids,* edited by Y. S. Touloukios and E. H. Buyco (Plenum, New York, 1970), p. 1325.

[14]G. F. Imbusch, Phys. Rev. **153**, 326 (1967).

[15]R. C. Powell, B. DiBartolo, B. Birang, and C. S. Naiman, Phys. Rev. **155**, 296 (1967).

[16]R. C. Powell and B. DiBartolo, Phys. Status Solidi A **10**, 315 (1972), and references therein.

[17]M. Inokuti and H. Hirayama, J. Chem. Phys. **43**, 1978 (1965).

[18]D. L. Huber, J. Lumin. **28**, 475 (1983).

[19]W. Platz and J. Heber, Z. Phys. B **24**, 333 (1976).

[20]J. P. van der Ziel, J. Chem. Phys. **57**, 2442 (1972).

[21]A. M. Ghazzawi, J. K. Tyminski, R. C. Powell, and J. C. Walling, Phys. Rev. B **30**, 7182 (1984).

[22]D. J. Harter, M. L. Shand, and Y. B. Band, J. Appl. Phys. **56**, 865 (1984).

[23]W. Jia, Y. S. Shang, R. M. Tang, and Z. Y. Yao, J. Lumin. **31-32**, 272 (1984).

[24]T. Kushida and M. Kikuchi, J. Phys. Soc. Jpn. **23**, 1333 (1967).

[25]T. Muramoto, Y. Fukuda, and T. Hashi, Phys. Lett. **48A**, 181 (1974).

[26]D. L. Dexter, J. Chem. Phys. **21**, 836 (1953).